

A climatology of stratospheric aerosol

Matthew H. Hitchman, Megan McKay,¹ and Charles R. Trepte²

Department of Atmospheric and Oceanic Sciences, University of Wisconsin - Madison

Abstract. A global climatology of stratospheric aerosol is created by combining nearly a decade (1979–1981 and 1984–1990) of contemporaneous observations from the Stratospheric Aerosol and Gas Experiment (SAGE I and II) and Stratospheric Aerosol Measurement (SAM II) instruments. One goal of this work is to provide a representative distribution of the aerosol layer for use in radiative and chemical modeling. A table of decadal average $1\ \mu\text{m}$ extinction values is included, extending from the tropopause to 35 km and 80°S to 85°N , which allows estimation of surface area density. We find that the aerosol layer is distinctly volcanic in nature and suggest that the decadal average is a more useful estimate of future aerosol loading than a “background” loading, which is never clearly achieved during the data record. This climatology lends insight into the general circulation of the stratosphere. Latitude - altitude sections of extinction ratio at $1\ \mu\text{m}$ are shown, averaged by decade, season, and phase of the quasi-biennial oscillation (QBO). A tropical reservoir region is diagnosed, with an “upper” and a “lower” transport regime. In the tropics above 22 km (upper regime), enhanced lofting occurs in the summer, with suppressed lofting or eddy dilution in the winter. In the extratropics within two scale heights of the tropopause (lower regime), poleward and downward transport is most robust during winter, especially in the northern hemisphere. The transport patterns persist into the subsequent equinoctial season. Ascent associated with QBO easterly shear favors detrainment in the upper regime, while relative descent and poleward spreading during QBO westerly shear favors detrainment in the lower regime. Extinction ratio differences between the winter-spring and summer-fall hemispheres, and differences between the two phases of the QBO, are typically 20–50%. Dynamical implications of the aerosol distributions are explored, with focus on interhemispheric differences, strong subtropical gradients, and the pronounced annual cycle.

1. Introduction

The optical and climatic effects of the stratospheric sulfuric acid aerosol layer have been written about for centuries [Turco *et al.*, 1979]. More recently, scientists have focused on its role in ozone chemistry [Cadle, 1975; Hofmann and Solomon, 1989; Stolarski and Wesoky, 1993]. Indeed, the massive eruption of Mount Pinatubo appears to have led to notable ozone decreases in the presence of anthropogenic chlorine [Prather, 1992; Bekki *et al.*, 1993; Herman *et al.*, 1993; Schoeberl *et al.*, 1993] as well as changes in the distribution of surface temperatures [Hansen *et al.*, 1992; Robock and Mao, 1992].

Stratospheric aerosol scatters solar radiation at $1\ \mu\text{m}$ effectively. This property has been used to measure the aerosol distribution with solar occultation instruments mounted on polar orbiting spacecraft [McCormick *et al.*, 1979]. A primary goal of the present work is to create a global stratospheric aerosol climatology using available satellite data of this type. The Stratospheric Aerosol and Gas Experiment (SAGE I and II) instruments [McCormick *et al.*, 1989] were designed to sample the tropics and midlatitudes, while the Stratospheric Aerosol Measurement (SAM II) instrument [Russell *et al.*, 1981] was designed to observe the polar regions. Many discrete volcanic eruptions occurred during the data record. In order to ensure meaningful spatial patterns, only contemporaneous polar and nonpolar data were included, yielding a total of 9 years and 1 month.

Trepte and Hitchman [1992] presented sample aerosol distributions during the westerly and easterly shear phases of the quasi-biennial oscillation (QBO). Their findings include a tropical reservoir, pronounced meridional gradients in the subtropics, and notably different patterns for the two phases of the QBO. Aerosol observations from satellite [McCormick and Veiga, 1992; Trepte *et al.*, 1993] and ground-based lidar [Langford,

¹Now at Department of Soil, Crop and Atmospheric Sciences, Cornell University, Ithaca, NY.

²Now at Science Applications International Corporation, Hampton, VA.

Copyright 1994 by the American Geophysical Union.

Paper number 94JD01525.
0148-0227/94/94JD-01525\$05.00

A. O., et al., Transport of the Pinatubo volcanic aerosol to a northern midlatitude site, submitted to *Journal of Geophysical Research*, 1994] have proven useful in diagnosing the transport of Mount Pinatubo debris out of the tropical reservoir. In this work we emphasize long-term averaging to enable a systematic climatological study of the relationship between aerosol and the general circulation. The satellite data and analysis methods are described in section 2, including screens, data frequency, and binning techniques for creating the decadal, quasi-biennial, and seasonal averages. Variability due to volcanic activity, the decadal average aerosol distribution, and the use of tabulated extinction values for stratospheric models are discussed in section 3. Implications for seasonal and quasi-biennial variations in the general circulation are described in sections 4 and 5, respectively. In the final section we focus on dynamical implications of the observed annual cycle, interhemispheric differences, and the pronounced meridional gradients flanking the tropical aerosol reservoir.

2. Satellite Data and Analysis Methods

2.1 General Considerations

The SAGE I and II and SAM II instruments measure extinction of solar radiation at $1 \mu\text{m}$ by scanning the solar disk as it rises and sets in polar orbit. Usually there are 28-30 profiles taken per day by each instrument. They generally extend from the tropopause (or below if it is clear) to 30 km (SAM II) or 40 km (SAGE), with 1 km vertical resolution. The reader is referred to McCormick et al. [1989] and Chu et al. [1989] for characteristics of the SAGE data, and to Russell et al. [1981] and Kent et al. [1985] for those of the SAM II data. Some aerosol reference profiles are given by McCormick et al. [1993].

A representative sampling pattern (1985) is shown in Figure 1. The SAM II instrument samples high latitudes, while the SAGE instruments sample tropical and midlatitudes. A seasonal average is the shortest period which ensures continuous latitudinal coverage. Even so, data gaps occur near 60° and the poles in the winter hemisphere (Figure 1). At seasonal and longer timescales, many features are primarily zonally symmetric. In this paper we concentrate on zonal mean phenomena. The data are binned every 5° of latitude from 80°S to 85°N and every kilometer from 8 to 35 km (but only to 30 km for the SAM II data).

In drawing dynamical conclusions from temporally averaged distributions, significance is much more readily established for spatially continuous features. The spatial and temporal discreteness of volcanic eruptions necessitated using only SAGE and SAM II data taken during the same months. The SAM II instrument has operated since February 1979. The SAGE I instrument operated from October 1978 to November 1981, while the SAGE II instrument has operated since October 1984. The months used in this climatology include February 1979 - November 1981 and October 1984 - De-

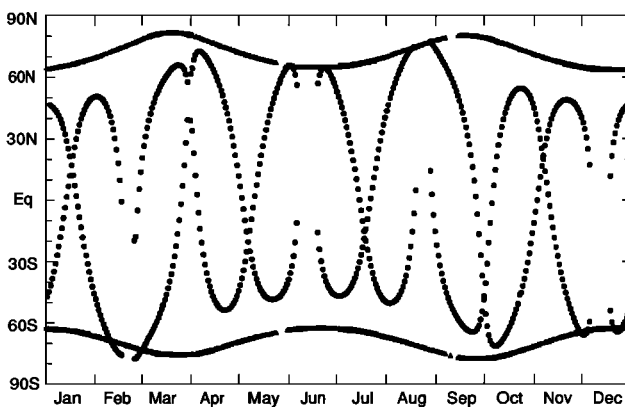


Figure 1. Time-latitude sampling pattern for SAM II (triangles, polar regions) and SAGE II (circles) during 1985. Each symbol represents the center of ~ 15 profiles for a given day. Note the poor sampling near 60°N and 85°N during the three-month season December, January, February and near 60°S and 85°N during the season June, July, August.

ember 1990, a total of 9 years and 1 month. Data since 1990 were excluded based on the historical observation that eruptions as large as Mount Pinatubo (June 1991) usually occur less often than once per decade.

A further decision in compiling the climatology was to try to exclude frozen particles. Along an aircraft flight path from $\sim 200 \text{ K}$ to $\sim 190 \text{ K}$ the composition of liquid droplets changes rapidly from sulfuric acid trihydrate to an increasing mixture of nitric acid trihydrate, then of water [e.g., Dye et al., 1992]. Near 190 K freezing and more rapid growth by water deposition occurs. Our decision to try to separate liquid aerosol from frozen grains is based in part on the course of developments in laboratory and model work. Laboratory studies have shown that the reactions which liberate chlorine and sequester nitrogen go much faster near grain boundaries than liquid surfaces, although in the range $190\text{--}195 \text{ K}$ this distinction may be less valid. Nevertheless, it has been traditional to treat frozen and liquid aerosols separately in numerical models. It is also easier to diagnose the general circulation from extinction ratio patterns when seasonally appearing frozen particles are excluded.

The types of data used include optical depth and profiles of extinction and extinction ratio at $1 \mu\text{m}$. During the data record, observed extinction values, E_o , are typically $10^{-4}\text{--}10^{-3} \text{ km}^{-1}$. If the particle size distribution is known, these may be converted to surface area density, S , the quantity most directly relevant for heterogeneous chemistry and radiative calculations (cf. section 3.3). Extinction ratio, β , is the ratio of aerosol extinction, E_a , to molecular extinction, E_m , estimated for gases alone [Russell et al., 1981]: $\beta = E_a/E_m$, where $E_a = E_o - E_m$. In the aerosol layer, values of β typically range from 0 to 35. Due to the effective normalization by air density, β is a useful indicator of aerosol amount to higher altitudes than extinction. Although microphysical processes exert an important influence on the distribution of aerosol, spatial differences in trans-

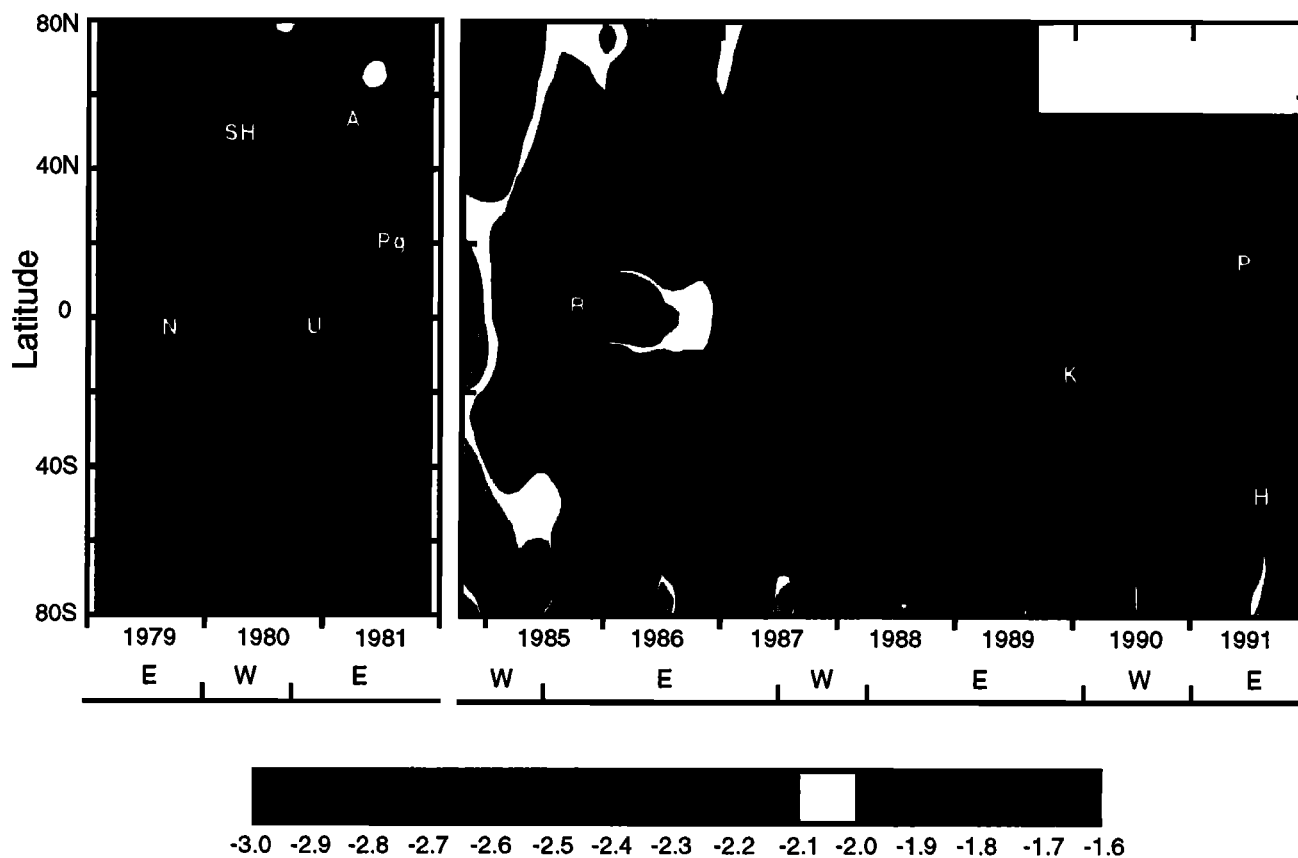


Plate 1. Time-latitude section of stratospheric aerosol optical depth at $1 \mu\text{m}$, blending SAGE I and II and SAM II data. The logarithm of optical depth is shaded for values less than -2.9 to greater than -1.7, with color change at interval 0.1. Letters indicate specific volcanic eruptions (see text). The dominant phase of the QBO is indicated below the time line, where W (E) indicates westerly (easterly) shear. SAM II data in the northern polar latitudes are unavailable after late 1989 because of gradual orbital precession.

port are effectively highlighted by patterns of extinction ratio. A latitude-time section of optical depth, the vertical integral of stratospheric extinction profiles, is used to show the distinct volcanic nature of the aerosol layer (Plate 1).

2.2 Screening and Averaging Methods

Five screens were used in processing the extinction and extinction ratio data. (1) A value was ignored if a profile was flagged as suspect. (2) It was also ignored if the estimated error exceeded 50%. (3) Values were ignored at and below where frozen particles were judged to be present. This was assumed for temperatures less than 198 K when a value exceeded the 80th percentile of nonwinter values [Kent *et al.*, 1985]. (4) A value was ignored as being contaminated by clouds if it was within 1 km of the tropopause level (provided with each profile) and exceeded 4.5 times the standard deviation plus the mean of binned values at that location. (5) In addition, nine SAGE (29 SAM II) profiles containing an extinction ratio value exceeding 100 (50) were ignored. All values shown were subjected to these screens, except for Plate 1, which represents frozen particles as well as liquid aerosol.

Average values were calculated for each 5° by 1 km bin on three timescales. The “decadal average” refers to the entire ~ 9.1 years of data. “DJF”, “MAM”, “JJA”, and “SON” refer to the three-month seasons beginning with December, January and February. Several different binning methods were assessed for highlighting aerosol differences between the easterly and westerly phases of the QBO. The method which best captures the phase differences is to bin according to the dominant sign of the vertical shear of zonal wind at Singapore (1°N , 104°E) in the layer 20-30 km. The periods chosen are as follows, where “QBO” in parentheses indicates where the aerosol data began or ended in the middle of a QBO phase: easterly shear, February 1979 (QBO) to June 1979, July 1980 to November 1981 (QBO), October 1985 to April 1987, March 1988 to July 1989, November 1990 to December 1990 (QBO); westerly shear, July 1979 to June 1980, October 1984 (QBO) to September 1985, May 1987 to February 1988, August 1989 to October 1990. They may be compared with the time-altitude section in Holton [1992, Figure 12.11, p. 427]. Out of the 109 months of data, 60 months (or 55% of the profiles) were assigned to the easterly shear category (westward winds increasing with

altitude), which is characterized by equatorial lofting. Westerly shear (49 months) is characterized by equatorial subsidence and meridional divergence in the lower stratosphere. In the figures to be shown, bins with fewer than 50 data values are left blank.

3. Decadal Average

3.1 Volcanic Variability

A latitude-time diagram of stratospheric optical depth at $1 \mu\text{m}$ is shown in Plate 1. This quantity was obtained by integrating extinction values from 2 km above the tropopause to 35 km (without screening out frozen particles). The combined SAGE and SAM II data shown here cover the time periods included in the climatology, plus 1991. Note the data gap of nearly 3 years between SAGE instruments. In addition, SAM II data in the northern polar latitudes are unavailable after late 1989 because of the gradual precession of the orbit. One may see the enhanced particle formation over the polar regions in winter. The range in optical depth is $\sim 0.001 - 0.02$, exclusive of Mount Pinatubo. Most notably, one can see the influence of the following eruptions indicated by the first letter: Negra (1°S , November 1979), Ulawun (5°S , October 1980), St. Helens (46°N , May 1980), Alaid (51°N , April 1981), Pagan (18°N , May 1981), Chichon in the data gap (17°N , April 1982), Ruiz (5°N , November 1985), Kelut (8°S , February 1990), Pinatubo (15°N , June 1991), and Hudson (46°S , August 1991). Aerosol from extratropical eruptions tends to be removed from the stratosphere more readily than from tropical eruptions. Note that tropical aerosol tends to be confined during QBO easterly shear (e.g., Ulawun and Ruiz) and summer, but spreads poleward more readily during QBO westerly shear (e.g., Kelut) and winter. These aspects of seasonal and quasi-biennial transport will be described more fully in sections 4 and 5.

Two conclusions may be drawn which are fundamental to this climatology:

1. The record is distinctly volcanic in nature, with a monotonic decrease in optical depth after each eruption. It is not clear that minimum equilibrium values were reached during this record; a new eruption always interrupted a downward trend. Globally integrated optical depth also shows the same signal of decrease interrupted by eruption [McCormick and Veiga, 1992, Figure 1]. This is also true of hemispherically integrated optical depth (Glenn Yue, personal communication, 1993). This suggests that a "background" aerosol distribution, due solely to conversion of precursor sulfur compounds wafting up from the troposphere, may be rare.

2. The degree of volcanic activity during the data record is broadly representative of volcanic activity over the past century. This statement is based on a qualitative inspection of variability in the volcanic explosivity index [Newhall and Self, 1982; Smithsonian Institution, 1989], sulfur emission index [Schnetzler et al., 1992],

and pyrhelimeter data [Goodman, 1984]. This ~ 9.1 year data record may be taken as a "best guess" for future decades which lack very large eruptions. Values ~ 10 times larger are appropriate for Mount Pinatubo. It is difficult to extrapolate to very large eruptions, such as that of Mount Toba $\sim 75,000$ years ago, which left a 65 km diameter lake in Sumatra [Wilson, 1992, p. 24].

3.2 Tropical Reservoir, Upper and Lower Transport Regimes

The decade average distribution of extinction ratio is shown in Figure 2. The number of values in each 5° by 1 km bin typically exceeds 10^3 and reaches 10^4 for the SAM II data in the polar regions. The pattern of standard deviation of these values (not shown) is very similar to Figure 2, with standard deviations being about 25% of extinction ratio values. Maximum tropical extinction ratio values are in the range 50-80 before filtering, but post-eruption values decay rather quickly. Near the aerosol maximum, the fourth screen (section 2.2) filtered out values exceeding ~ 40 .

This decadal average distribution reveals the integrated transport effects on many eruptions. One may infer from Figure 2 that aerosol from extratropical eruptions is removed from the stratosphere more quickly than from tropical eruptions, leaving a characteristic maximum over the equator near 21 km. Here aerosol extinction exceeds molecular extinction by a factor of ~ 12 , with values decreasing monotonically upward to 35 km and poleward and downward to the extratropical tropopause near 8 km. For any subperiod the pattern is similar. The decrease downward to the tropopause, below which there are no contours, may be ascribed to sedimentation, dilution by tropospheric air, and insufficient ultraviolet light for photolyzing precursor sulfur species.

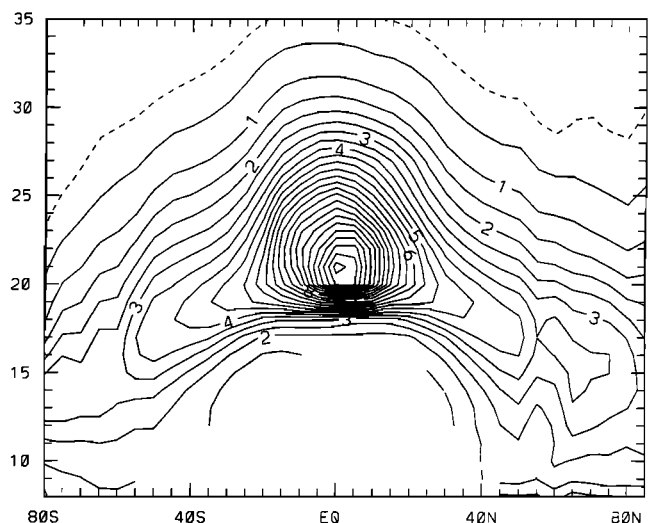


Figure 2. Latitude-altitude section of extinction ratio at $1 \mu\text{m}$ averaged for the ~ 9.1 years of contemporaneous SAGE and SAM II data, with a contour interval of 0.5 and dashed line at 0.25.

Above the dashed contour in Figure 2 aerosol extinction is less than one quarter of molecular extinction. This upward decrease is probably due to evaporation as air experiences net radiative heating and ascends. It is likely that the liquid aerosol contains solid cores [Turco *et al.*, 1979]. It may be of interest to investigate whether the cores could nucleate new droplets upon arrival in cold polar regions. Hofmann and Rosen [1984] have shown that, following the eruption of El Chichon in April 1982, a surge in particles with radius less than 0.01 μm occurred above 29 km over Laramie, Wyoming in January 1983. They showed that this air came over the north pole between the Aleutian High and displaced polar vortex. In a study of the climatology of the Aleutian High (M. H. Hitchman and V. L. Harvey, manuscript in preparation) it has been shown that this type of air motion can be traced back further around the polar vortex to the eastern hemisphere subtropics. This topic will be returned to in conjunction with the seasonal cycle.

Aerosol gradients are more pronounced beginning near the 5 contour. The region bounded roughly by the 5 contour may be regarded as a reservoir of tropical stratospheric air which is partially sequestered from the rest of the stratosphere. Relatively high values are found in a column above 22 km over the tropics (the "upper regime") and in the extratropics within ~ 10 km of the tropopause (the "lower regime"). In the decadal average, lofting in the upper regime is more pronounced in the southern subtropics, while poleward and downward transport in the lower regime is stronger in the northern hemisphere. As will be shown in section 4, this is due to the more vigorous circulation present during the northern winter and spring.

The pronounced meridional gradient near 20°N and S is a striking, persistent feature of the aerosol pattern. For the lower transport regime to exist, some mixing must occur across the subtropics. We infer that this mixing is simply weaker than in the extratropics, where gradients are seen to be significantly weaker. This conclusion was also reached by Murphy *et al.* [1993] in explaining remarkably strong subtropical gradients in the ratio of reactive nitrogen to ozone seen in ER-2 flights.

The location of enhanced gradients in some constituents on the winter hemisphere side may be close to the equatorward edge of a region of pronounced mixing, or "surf zone" [McIntyre and Palmer, 1984], where it has been hypothesized that a "semipermeable barrier" to transport exists, which is due to an enhanced meridional gradient of potential vorticity [McIntyre, 1990]. On the other hand, the aerosol gradient on the summer hemisphere side coincides with a region of strong shear associated with the subtropical easterly jet. The nature of this transport barrier will be explored further in section 6.

3.3 Tabulated Extinctions and Model Usage

The decadal average values of observed extinction, E_o , are given in Table 1, with a 2 km by 10° resolution. We have made the decadal, quasi-biennial and seasonal values at 1 km by 5° resolution available electronically (write to User and Data Services, Distributed Active Archive Center, MS 157B, NASA Langley Research Center, Hampton, VA 23681). From these values, surface area density (S) may be calculated. At present, this conversion contains a great deal of uncertainty, due to the relative lack of knowledge of the global variation of aerosol size distributions and their evolution following an eruption. Thomason and Poole [1993] have recently employed other SAGE II channels to infer size distributions. In separate work we are studying the effects of aerosol on ozone, using a two-dimensional model which is described by Brasseur *et al.* [1990]. The conversion method we use is based on the data of Jäger and Hofmann [1991], who performed extensive lidar and particle counter measurements over Wyoming. Ratios of surface area density to backscatter, and observed extinction to backscatter, varied considerably during their observation period 1980-1987 and over their altitude bins 15-20, 20-25 and 25-30 km. We fitted a vertical profile to the average of their ratios during the periods 1980-1981 and 1985-1987, which were contemporaneous with the satellite aerosol data. The resulting formula for converting observed aerosol extinction, E_o , tabulated in units of km^{-1} , to surface area density, S , in units

Table 1. Decadal Mean Values of Aerosol Extinction at 1 μm , in Units of 10^{-4} km^{-1} , Given Every 10° From 80°S to 80°N and Every 2 km From 8 km (or the Tropopause) to 34 km Altitude.

	80°S	70°S	60°S	50°S	40°S	30°S	20°S	10°S	0°	10°N	20°N	30°N	40°N	50°N	60°N	70°N	80°N
34	.01	.01	.02	.02	.02	.02	.03	.04	.04	.03	.03	.02	.02	.02	.02	.01	.01
32	.01	.02	.02	.03	.03	.04	.06	.09	.09	.07	.06	.04	.03	.03	.02	.02	.02
30	.05	.05	.04	.04	.05	.08	.14	.22	.24	.20	.14	.08	.05	.05	.03	.05	.06
28	.05	.08	.07	.08	.12	.18	.34	.56	.66	.57	.37	.18	.11	.09	.06	.08	.10
26	.08	.13	.14	.20	.29	.42	.74	1.3	1.5	1.3	.80	.42	.26	.21	.13	.16	.16
24	.15	.25	.28	.48	.66	.87	1.5	2.6	3.1	2.5	1.5	.88	.60	.47	.33	.34	.28
22	.31	.47	.56	1.0	1.3	1.7	2.6	4.3	5.5	4.7	3.0	1.8	1.3	1.0	.76	.70	.54
20	.62	.91	1.1	2.0	2.5	3.1	4.0	5.5	8.1	6.7	4.4	3.2	2.6	2.1	1.7	1.6	1.2
18	1.0	1.7	2.0	3.3	3.7	3.9	3.3	3.2	2.9	2.8	3.2	4.1	4.1	3.6	3.1	2.6	2.4
16	2.1	2.8	3.1	4.2	3.8	2.8	2.1	2.1	2.7	2.5	2.3	3.0	4.4	4.8	4.1	4.4	4.1
14	4.8	4.5	3.9	4.2	3.3	2.5					1.7	2.8	4.2	5.3	4.6	5.8	5.4
12	5.6	5.3	4.6	4.5	3.8	2.6						3.0	5.0	6.0	5.7	7.1	6.6
10	5.3	5.6	5.7	5.3	5.1	3.4						4.0	7.1	7.7	8.6	7.9	7.8
8	3.9	5.0	5.1	5.0	6.7								6.0	5.8	6.6	5.9	6.1

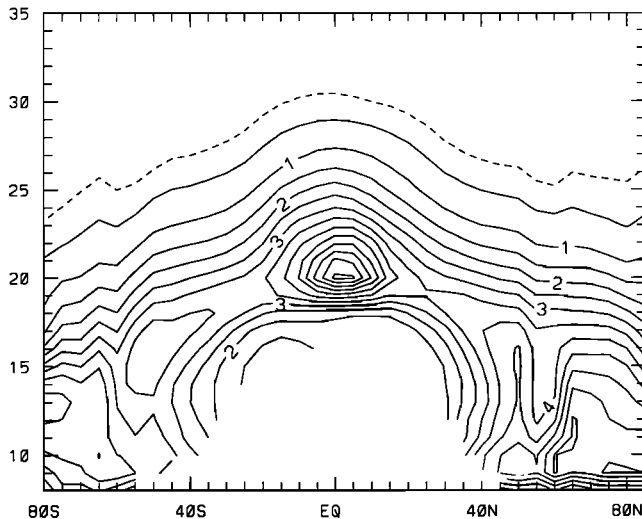


Figure 3. As in Figure 2, except for aerosol surface area density in square microns per cubic centimeter, using the conversion factor given by equation (1).

of $\mu\text{m}^2 \text{cm}^{-3}$, increases linearly above the tropopause, Z_T , which varies with latitude:

$$S(y, z) = \left[0.8 \left(\frac{Z - Z_T(y)}{20} \right) + 0.7 \right] \times 10^4 \times E_o(y, z). \quad (1)$$

In Table 1 Z_T is the lowest altitude that is not blank. The standard deviation of the conversion factor in Jäger and Hofmann's data is about 1/3 of the values in (1). The sensitivity of model results to uncertainties in conversion factor may be estimated by halving or doubling surface area densities.

Figure 3 shows the decade average pattern of surface area density using (1). Due to the lack of normalization by air density, maximum values of surface area density are found at lower altitudes than for extinction ratio. Within 5 km of the tropopause, surface area values are estimated to be about $3 \mu\text{m}^2 \text{cm}^{-3}$ on the decadal average, exceeding 5 in the tropics and north polar regions. These values are about 10 times larger than the 1979 values used in current ozone assessment models [Prather *et al.*, 1992; Stolarski and Wesoky, 1993]. We feel that the decadal averages are a better estimate of future aerosol loading. As an example of the significance of aerosol, in our two-dimensional model the effects of nitrogen emissions from a proposed fleet of high speed civil transports are largely negated through sequestering in the aerosol (results to be reported elsewhere).

4. Seasonal Averages

Extinction ratio distributions for boreal winter (DJF), spring (MAM), summer (JJA), and fall (SON) are shown in Figure 4. The percent interhemispheric differences for each season are shown in Figure 5. The number of measurements at each point in these plots is about 1/4 that of the decadal average, with notable exceptions due to the changing sampling pattern (Figure 1). Bins con-

taining fewer than 50 values were left blank in Figures 4 and 5: 55°N, 60°N and 85°N during DJF, and 55°S, 60°S, 80°S, and 85°N during JJA. Within each season the aerosol distribution is again nearly continuous, with values decreasing monotonically away from the 21 km level over the equator.

The overall impression is a stretching of contours upward in the summer subtropics, simultaneously with poleward and downward stretching in the winter (Figures 4a and 4c). The same contour pattern is present in the subsequent equinoxes: upward displacement in the fall hemisphere, with poleward and downward displacement in the spring (Figures 4b and 4d). In each season values in the region 25-33 km, equatorward of 40° are high in the summer and fall, and low in the winter and spring (Figure 5), with typical interhemispheric differences being ~20-40%. In the layer 8-25 km, high values extend poleward and downward out of the tropics quite markedly in the northern winter and spring (Figure 4). During northern winter and spring values are 20-50% larger than in the southern hemisphere in the lower transport regime, with this difference increasing toward the pole (Figures 5a and 5b). The layer of enhanced aerosol over high northern latitudes is quite deep in spring (Figure 4b). During the southern hemisphere winter and spring, values are higher than in the northern summer and fall by 10-20% (Figures 5c and 5d), but only to ~50° latitude. Poleward of this, aerosol amounts are much lower in southern winter and spring, consistent with pronounced descent of aerosol-poor air over Antarctica at these levels. This likely occurs through gravity wave driven descent in the upper stratosphere [Hitchman *et al.*, 1989], strong radiative cooling by exchange with the cold elevated Antarctic and space, and a lack of strong quasi-horizontal mixing relative to the north polar winter vortex.

Aerosols share a notable characteristic with other tracers in that maximum displacement occurs when transport is waning. Hence the similarity of the equinox patterns to the preceding solstice patterns (Figures 5a-5b and 5c-5d) does not necessarily indicate similarly vigorous transport. Recall that column ozone amounts maximize in accumulation regions over northern high latitudes and southern midlatitudes in spring.

The tropical confinement of aerosol and its implied local minimum in transport suggest a modification to the Brewer-Dobson circulation model. This model has emerged through consideration of the water vapor budget [Brewer, 1949], column ozone distribution [Dobson, 1956], the radiative budget [Murgatroyd and Singleton, 1961], the dispersal of radioactive tracers from bomb tests in the 1950s and 1960s [Feely and Spar, 1960; Tellegadas and List, 1969], and the pattern of diminution of solar radiation at the surface after the eruption of Mount Agung in March 1963 [Dyer and Hicks, 1968]. It is tempting to infer from Figures 4 and 5 that the lower transport regime of the Brewer-Dobson circulation is unidirectional. Yet the aerosol maximum is nearly always over the equator soon after an eruption. Interestingly, a year after a bomb was exploded near 12°N,

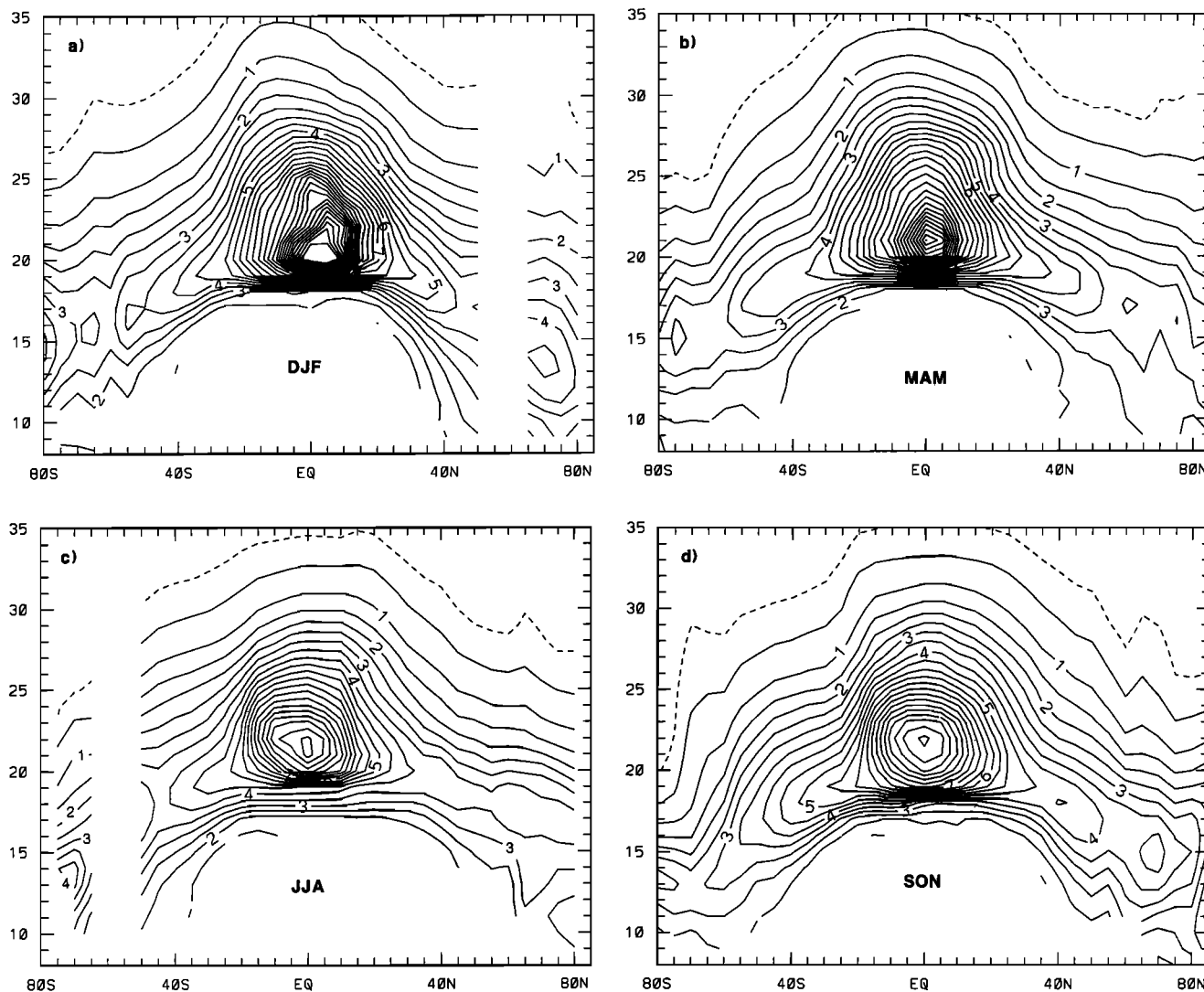


Figure 4. As in Figure 2, except averaged by season: (a) DJF, (b) MAM, (c) JJA, (d) SON.

21 km in 1958, radioactive debris concentrations maximized over the equator, with a poleward and downward plume similar to that in the aerosol distributions [Feely and Spar, 1960]. This suggests that the lower transport regime involves two-way stirring, but with a bias toward poleward and downward transport. Given an equatorward decrease in mixing rates, debris from an extratropical eruption could reach the tropics, while extratropical material is removed more rapidly, leaving a much smaller relative maximum over the equator months later.

Other evidence supporting two-way transport comes from recent observations of water vapor [Tuck *et al.*, 1993]. During the Antarctic spring of 1992 low water vapor values from the south polar vortex appeared to reach the tropics. Another curious observation is the very weak meridional gradient in ozone compared to aerosol in the subtropical lower stratosphere [Trepte, 1993]. This could be explained by the fact that the source of ozone is distributed across the transport minimum. The distribution and apparent direction of trans-

port for a particular constituent must depend on the relative strengths and locations of sources and sinks.

As another example, in the upper transport regime more aerosol is found in the summer than in the winter subtropics and the pattern is most notable during the northern winter (Figures 4 and 5). Is this due purely to enhanced lofting from the tropical reservoir on the summer hemisphere side, or is there a significant contribution to this pattern by removal of aerosol-rich air and injection of aerosol-poor air from the winter extratropics? The Aleutian High and displaced polar vortex are robust features of the northern winter circulation. This vortex pair tilts westward with altitude and yields a chronic zonal asymmetry in low latitudes. In the layer 25–35 km, during most winter days extratropical air enters the tropics in the western hemisphere, while tropical air moves poleward in the eastern hemisphere. Since polar air is depleted in aerosol, due to subsidence from aloft, this horizontal mixing pattern is likely to be equally as important as summer ozone heating in accounting for the shape of the upper regime.

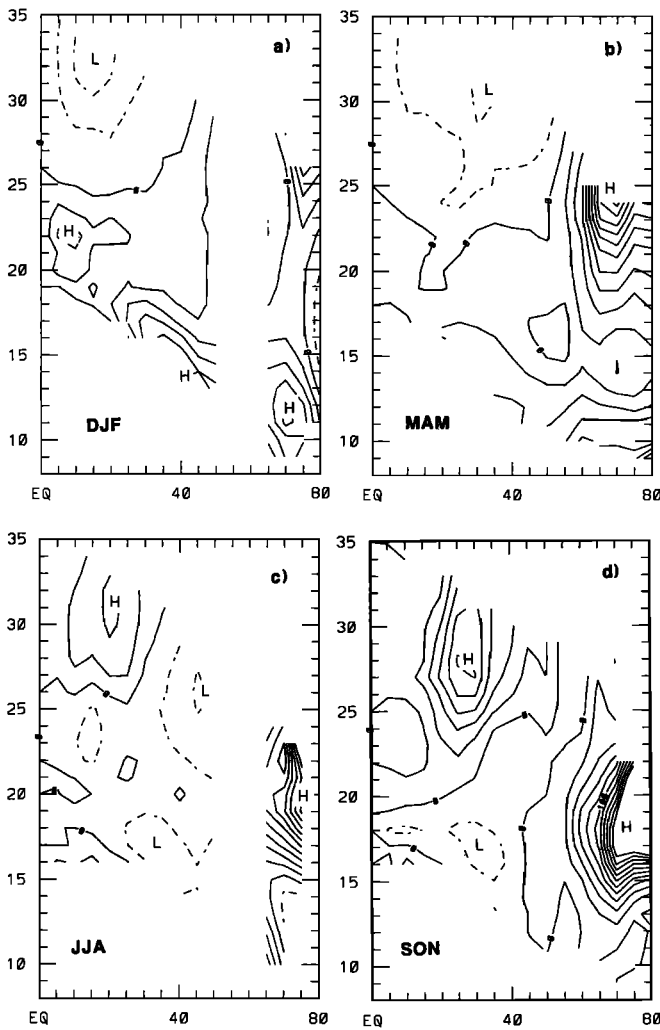


Figure 5. Latitude-altitude section of the hemispheric difference in seasonal average extinction ratio expressed in percent; $(N - S)/S \times 100$, with contour interval 20%, for (a) DJF, (b) MAM, (c) JJA, (d) SON. Negative values (dashed) indicate that southern hemisphere values are higher for a given three-month averaging period.

5. QBO Variations

The aerosol distribution also varies markedly with the phase of the QBO. Figure 6 shows extinction ratios binned according to times of predominant westerly and easterly shear, while Figure 7 shows the percent difference (westerly minus easterly). The overall impression is a gathering and lofting during the easterly shear phase and a slumping and poleward spreading during westerly shear. Extinction ratio values are higher by 25-50% in the upper regime during easterly shear and by 25-50% in the lower regime during westerly shear. This result is consistent with expectations from theory and models [e.g., *Plumb and Bell, 1982*]. In easterly shear and near an equatorial easterly wind maximum, easterly wave driving leads to poleward flow (divergence) and ascent from below. In westerly shear and near a westerly wind maximum, westerly wave driving leads

to equatorward flow (convergence) with descent below. Thus, an easterly shear layer is characterized by ascending air with meridional convergence at the base, while a westerly shear layer is characterized by descending air and meridional divergence at the base. The comments in section 4 regarding maximum displacement of material when transport is waning also apply to the descending shear zones of the QBO. The strongest meridional divergence occurs at the level of maximum easterlies, so the maximum poleward displacement may be expected when westerly shear is present. These circulations expected from theory are revealed quite clearly in the aerosol patterns shown in Figures 6 and 7.

These patterns suggest that, in the upper regime, air is made more accessible for detrainment from the tropical reservoir in the upper stratosphere during QBO easterly shear. In the lower regime air is more readily available for transport into the polar lower stratosphere during westerly shear. Optical depth primarily represents aerosol in the lower stratosphere. A careful

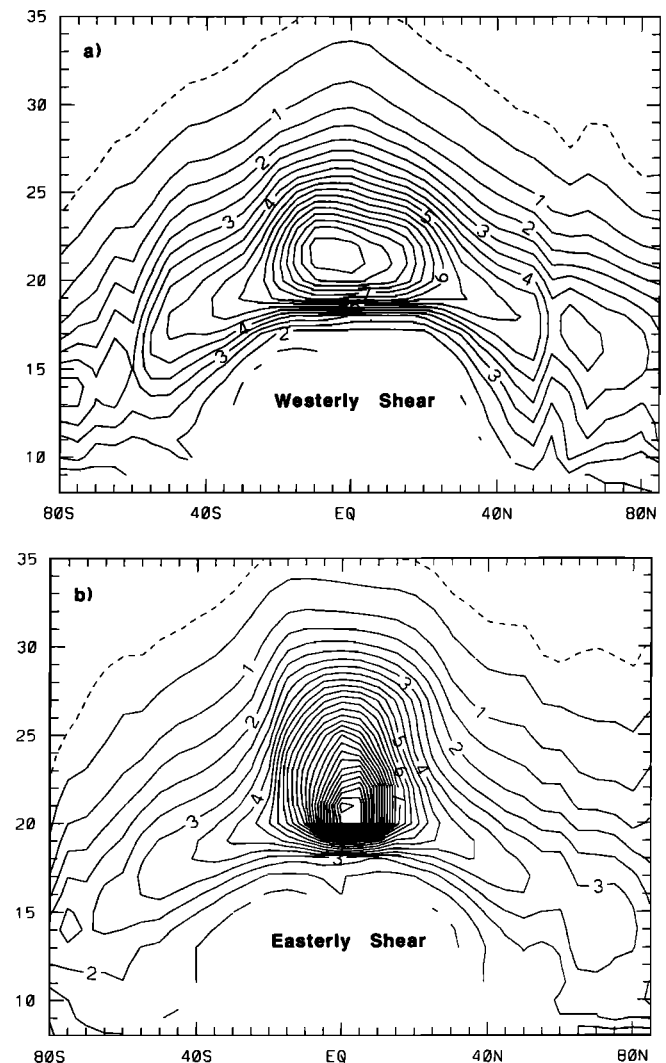


Figure 6. As in Figure 2, except averaged by phase of the QBO, as determined by predominant (a) westerly shear or (b) easterly shear of zonal wind at Singapore (see text).

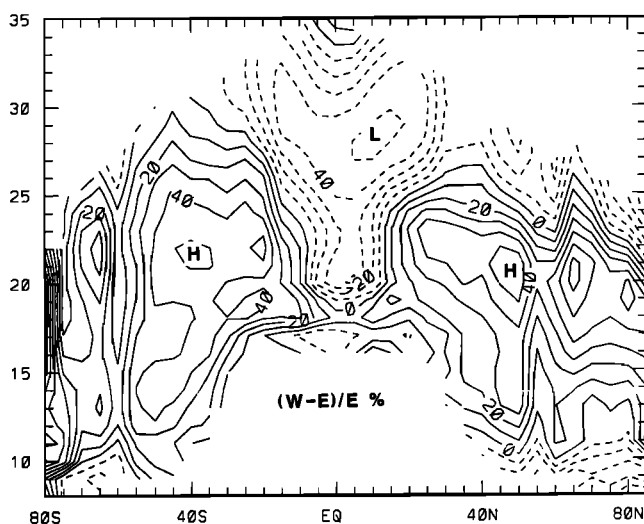


Figure 7. Latitude-altitude section of the percent difference in extinction ratio between the westerly shear and easterly shear phases of the QBO: $(W - E)/W \times 100$, with contour interval 10%. Dashed contours indicate values which are higher during periods of predominant easterly shear.

inspection of Plate 1 verifies that poleward transport of tropical aerosol in the lower regime occurs more readily during QBO westerly shear and in the winter and spring.

Aerosol changes of the order 25-50% might be expected to exert a noticeable influence on stratospheric chemistry and the local stratospheric heat budget [Labitzke and McCormick, 1992]. Other phenomena which might be modulated by quasi-biennial variations in aerosol loading include seeding of cirrus clouds and the meridional distribution of total radiation and of biologically active ultraviolet radiation at the surface.

6. Discussion

6.1 Summary

This climatology provides the first global view of long-term average aerosol distributions on decadal, quasi-biennial, and seasonal timescales. It strongly supports the notion that the aerosol layer is fundamentally volcanic in nature, with the general circulation preserving tropical debris longer, creating a reservoir. It also provides decadal average extinction values for use in modeling the current and future states of the stratosphere.

Detrainment from the tropical reservoir may be divided into an "upper" and a "lower" regime, where ascent occurs above 22 km in the tropics, with simultaneous poleward and downward transport closer to the tropopause. The pattern of aerosol displacement is strongest in northern winter and spring. The lower transport regime does not appear to penetrate the south polar vortex, consistent with subsiding aerosol-poor air. In the upper regime, ozone heating enhances lofting on the summertime, while dilution by planetary wave transport occurs on the wintertime. During the northern win-

ter, organized transport by the Aleutian High and the displaced polar vortex brings tropical air poleward in the eastern hemisphere and polar air equatorward in the western hemisphere. The reduced aerosol amounts in the winter subtropics near the top of the evaporating tropical aerosol plume may therefore be related to small particle surge events such as those reported by Hofmann and Rosen [1984].

A striking difference also exists between the easterly and westerly shear phases of the QBO, with enhanced tropical confinement and lofting during the easterly shear phase, and with subsidence and enhanced poleward and downward transport during the westerly shear phase. The global aerosol distributions provide a useful constraint on atmospheric motions. We are currently pursuing quantification of such motions through the use of an aerosol microphysical model. Two dynamical features bear further consideration here: the sharpness of the subtropical gradient and the nature of the annual cycle in the lower transport regime.

6.2 Subtropical Gradients

The sharpness of the subtropical gradient in aerosol is evidence of regions of reduced transport, which should be included in numerical models. But what is the dynamical explanation for this "transport barrier"? An examination of climatological distributions of zonal mean zonal wind and potential vorticity (PV) gradient proves to be useful [e.g., Randel, 1992, pp. 165, 171]. Large PV gradients can suppress irreversible mixing by breaking Rossby waves. Near 50 hPa (~ 22 km) a pronounced PV gradient occurs near 60° in the winter hemisphere on the poleward edge of the "surf zone", but it is difficult to see any enhancement of the PV gradient in the subtropics. In the summer subtropics, pronounced meridional shear of the zonal flow occurs on the flanks of the easterly jet, which tends to coincide with climatological aerosol gradients. The concept of shear suppression of eddy transport has emerged through conversations with David Newman, Paul Terry, and Andrew Ware. The basic notion is that sufficiently strong shear will elongate eddies to the point of destruction before they have time to rotate and transport constituents. This mechanism of shear suppression of eddy transport and geophysical applications are discussed by A. S. Ware et al. (The role of shear in geophysical transport barriers, submitted to *Geophysical Research Letters*, 1994).

6.3 Annual Cycle

Poleward transport within the lower regime likely involves mixing by Rossby waves [e.g., Rosenlof and Holton, 1993], inertio-gravity waves [Palmer et al., 1986; Iwasaki et al., 1989] and quasi-stationary monsoon structures in the summer subtropics [M. H. Hitchman and G. A. Postel, manuscript in preparation]. In conjunction with pronounced seasonal changes in aerosol, the tropopause throughout the entire tropics undergoes a surprising annual cycle, with the tropopause being highest and coldest in February and lowest and warmest in August [Reed, 1962; Reed and Vlcek, 1969; Reid and

Gage, 1981, 1985]. The annual variation in the strength of this circulation, being upward through the tropical tropopause, then poleward and downward into the winter hemisphere, has been ascribed to lower stratospheric wave driving being more pronounced during the northern winter [Robinson, 1980; Holton, 1990; Follows, 1992; Yulaeva et al., 1994]. An annual cycle in tropical convection may also play a role. Mitchell and Wallace [1992] showed that outgoing longwave radiation averaged from 6°S to 6°N is higher during northern summer. They ascribed the associated reduction in convection to the seasonal development of equatorial cold tongues in the eastern Pacific and Atlantic during northern summer. Moreover, the deepest convection might be expected during northern winter due to the destabilizing influence of east Asian cold air outbreaks near Indonesia. Zhang [1993] found that the mean fractional cloud cover for deep tropical clouds is largest during northern winter.

In order for air to undergo this zonal mean meridional circulation, it must cross potential temperature surfaces upward in the tropics and downward in the extratropics. It must also cross angular momentum surfaces, gaining westerly angular momentum during equatorward motion in the troposphere, and losing angular momentum during poleward flow in the stratosphere. Wave driving in the stratosphere allows parcels to move poleward, but this alone cannot explain how parcels move upward across potential temperature surfaces in the tropics. Nor can it explain the manner in which air gains angular momentum in trade easterlies or how air descends through potential temperature surfaces in the extratropics. Focusing on tropical entry into the stratosphere, the preponderance of evidence suggests that this occurs in preferred regions of active convection over warm surfaces, most notably near Indonesia. Air parcels must cool and become dehydrated, yet warm and ascend. Parcel motions in the vicinity of convective complexes are therefore quite complex. We are only beginning to understand the precise manner in which air enters the stratosphere. Nevertheless, evidence suggests that warmer sea surface temperatures tend to result in more air entering the stratosphere. From a zonal mean perspective, any change in tropical convection, stratospheric wave driving, extratropical subsidence, or subtropical lower tropospheric flow would change the meridional circulation. Since ascent into the stratosphere occurs preferentially near tropical convective centers, it is of interest to examine the geographical variation in the relationship between convective regions and poleward transport. Our work (to be reported elsewhere) shows that tropical-extratropical exchange occurs in preferred longitude bands near convective regions. These longitudinally isolated monsoon structures yield zonal mean Eliassen-Palm flux divergences which are compatible with the generation of wave activity (zonal asymmetries) by convection in the tropical lower stratosphere.

Acknowledgments. We would like to acknowledge interesting conversations with Ken Gage, Peter Haynes, Michael

McIntyre, Donal O'Sullivan, Adrian Tuck, Ron Woodman, and Yuk Yung. We also acknowledge the support of NASA grants NAG-1-1403, NAGW-2943, and NAS1-19958 during the course of this work.

References

- Bekki, S., R. Toumi, and J. A. Pyle, Role of sulphur photochemistry in tropical ozone changes after the eruption of Mount Pinatubo, *Nature*, **362**, 331-333, 1993.
- Brasseur, G., M. H. Hitchman, S. Walters, M. Dymek, E. Falise, and M. Pirre, An interactive chemical dynamical radiative two-dimensional model of the middle atmosphere, *J. Geophys. Res.*, **95**, 5639-5655, 1990.
- Brewer, A. W., Evidence for a world circulation provided by the measurements of helium and water vapor distribution in the stratosphere, *Q. J. R. Meteorol. Soc.*, **75**, 351-363, 1949.
- Cadle, R. D., Volcanic emission of halides and sulfur compounds to the troposphere and stratosphere, *J. Geophys. Res.*, **80**, 1650-1652, 1975.
- Chu, W. P., M. P. McCormick, J. Lenoble, C. Brogniez, and P. Pruvost, SAGE II inversion algorithm, *J. Geophys. Res.*, **94**, 8339-8352, 1989.
- Dobson, G. M. B., Origin and distribution of the polyatomic molecules in the atmosphere, *Proc. R. Soc. London, A*, **236**, 187-193, 1956.
- Dye, J. E., D. Baumgardner, B. W. Gandrud, S. R. Kawa, K. K. Kelly, M. Loewenstein, G. V. Ferry, K. R. Chan, and B. L. Gary, Particle size distributions in Arctic polar stratospheric clouds, growth and freezing of sulfuric acid droplets, and implications for cloud formation, *J. Geophys. Res.*, **97**, 8015-8034, 1992.
- Dyer, A. J., and B. B. Hicks, Global spread of volcanic dust from the Bali eruption of 1963, *Q. J. R. Meteorol. Soc.*, **94**, 545-554, 1968.
- Feely, H. W., and J. Spar, Tungsten-185 from nuclear bomb tests as a tracer for stratospheric meteorology, *Nature*, **188**, 1062-1064, 1960.
- Follows, M. J., On the cross-tropopause exchange of air, *J. Atmos. Sci.*, **49**, 879-882, 1992.
- Goodman, B. M., The climatic impact of volcanic activity, Ph.D. dissertation, 242 pp., Univ. of Wis. - Madison, 1984.
- Hansen, J., A. Lacis, R. Ruedy, and M. Sato, Potential climate impact of Mount Pinatubo eruption, *Geophys. Res. Lett.*, **19**, 215-218, 1992.
- Herman, J. R., R. McPeters, and D. Larko, Ozone depletion at northern and southern latitudes derived from January 1979 to December 1991 TOMS data, *J. Geophys. Res.*, **98**, 12,783-12,794, 1993.
- Hitchman, M. H., J. C. Gille, C. D. Rodgers, and G. Brasseur, The separated polar winter stratopause: A gravity wave driven climatological feature, *J. Atmos. Sci.*, **46**, 410-422, 1989.
- Hofmann, D. J., and J. M. Rosen, Balloon-borne particle counter observations of the El Chichon aerosol layers in the 0.01-1.8 μm radius range, *Geophys. Int.*, **23**, 155-185, 1984.
- Hofmann, D. J., and S. Solomon, Ozone destruction through heterogeneous chemistry following the eruption of El Chichon, *J. Geophys. Res.*, **94**, 5029-5041, 1989.
- Holton, J. R., On the global exchange of mass between stratosphere and troposphere, *J. Atmos. Sci.*, **47**, 392-395, 1990.
- Holton, J. R., *An Introduction to Dynamic Meteorology*, 3rd Edition, 507 pp., Academic, San Diego, Calif., 1992.
- Iwasaki, T., S. Yamada, and K. Tada, A parameterization scheme of orographic gravity wave drag with two different

- vertical partitionings, II: Zonally averaged budget analyses based on transformed Eulerian mean method, *J. Meteorol. Soc. Jpn.*, **67**, 29-40, 1989.
- Jäger, H., and D. Hofmann, Midlatitude lidar backscatter to mass, area, and extinction conversion model based on in situ aerosol measurements from 1980 to 1987, *Appl. Opt.*, **30**, 127-138, 1991.
- Kent, G. S., C. R. Trepte, U. O. Farrukh, and M. P. McCormick, Variation in the stratospheric aerosol associated with the north cyclonic polar vortex as measured by the SAM II satellite sensor, *J. Atmos. Sci.*, **42**, 1536-1551, 1985.
- Labitzke, K., and M. P. McCormick, Stratospheric temperature increases due to Pinatubo aerosols, *Geophys. Res. Lett.*, **19**, 207-210, 1992.
- McCormick, M. P. and R. E. Veiga, SAGE II measurements of early Pinatubo aerosols, *Geophys. Res. Lett.*, **19**, 155-158, 1992.
- McCormick, M. P., P. Hamill, T. J. Pepin, W. P. Chu, T. J. Swissler, and L. R. McMaster, Satellite studies of the stratospheric aerosol, *Bull. Am. Meteorol. Soc.*, **60**, 1038-1046, 1979.
- McCormick, M. P., J. M. Zawodny, R. E. Veiga, J. C. Larsen, and P. H. Wang, An overview of SAGE I and SAGE II ozone measurements, *Planet. Space Sci.*, **37**, 1567-1586, 1989.
- McCormick, M. P., P.-H. Wang, and M. C. Pitts, Background stratospheric aerosol and polar stratospheric cloud reference models, *Adv. Space Res.*, **13**, 7-29, 1993.
- McIntyre, M. E., Middle atmosphere dynamics and transport: Some current challenges to our understanding, in *Dynamics, Transport, and Photochemistry of the Middle Atmosphere*, pp. 1-18, Kluwer, Academic, Norwell, Mass., 1990.
- McIntyre, M. E., and T. N. Palmer, The "surf zone" in the stratosphere, *J. Atmos. Terr. Phys.*, **46**, 825-849, 1984.
- Mitchell, T. P. and J. M. Wallace, The annual cycle in equatorial convection and sea surface temperature, *J. Clim.*, **5**, 1140-1156, 1992.
- Murgatroyd, R. J., and F. Singleton, Possible meridional circulation in the stratosphere and mesosphere, *Q. J. R. Meteorol. Soc.*, **87**, 125-135, 1961.
- Murphy, D. M., D. W. Fahey, M. H. Proffitt, S. C. Liu, K. R. Chan, D. S. Eubank, S. R. Kawa, and K. K. Kelly, Reactive nitrogen and its correlation with ozone in the lower stratosphere and upper troposphere, *J. Geophys. Res.*, **98**, 8751-8773, 1993.
- Newhall, G. C., and S. Self, The volcanic explosivity index (VEI): An estimate of explosive magnitude for historical volcanism, *J. Geophys. Res.*, **87**, 1231-1238, 1982.
- Palmer, T. N., G. J. Shutts, and R. Swinbank, Alleviation of a systematic westerly bias in general circulation and numerical weather prediction models through an orographic gravity wave drag parameterization, *Q. J. R. Meteorol. Soc.*, **112**, 1001-1039, 1986.
- Plumb, R. A., and R. C. Bell, A model of the quasi-biennial oscillation on an equatorial beta-plane, *Q. J. R. Meteorol. Soc.*, **108**, 335-352, 1982.
- Prather, M., Catastrophic loss of stratospheric ozone in dense volcanic clouds, *J. Geophys. Res.*, **97**, 10,187-10,191, 1992.
- Prather, M. J. et al. (Eds.), The atmospheric effects of stratospheric aircraft: A first program report, *NASA Ref. Publ. 1272*, 233 pp., Office of Space Sci. and Appl., Washington, D. C., 1992.
- Randel, W. J., Global atmospheric circulation statistics, 1000-1 mb, *NCAR Tech. Note 366*, 256 pp., Natl. Center for Atmos. Res., Boulder, Colo., 1992.
- Reed, R. J., Some features of the annual temperature regime in the tropical stratosphere, *Mon. Weather Rev.*, **90**, 211-215, 1962.
- Reed, R. J., and C. L. Vlcek, The annual temperature variation in the lower tropical stratosphere, *J. Atmos. Sci.*, **26**, 163-167, 1969.
- Reid, G. C., and K. S. Gage, On the annual variation in height of the tropical tropopause, *J. Atmos. Sci.*, **38**, 1928-1938, 1981.
- Reid, G. C., and K. S. Gage, Interannual variations in the height of the tropical tropopause, *J. Geophys. Res.*, **90**, 5629-5635, 1985.
- Robinson, G. D., The transport of minor atmospheric constituents between troposphere and stratosphere, *Q. J. R. Meteorol. Soc.*, **106**, 227-253, 1980.
- Robock, A., and J. Mao, Winter warming from large volcanic eruptions, *Geophys. Res. Lett.*, **19**, 2405-2408, 1992.
- Rosenlof, K. H., and J. R. Holton, Estimates of the stratospheric residual circulation using the downward control principle, *J. Geophys. Res.*, **98**, 10,465-10,479, 1993.
- Russell, P. B., et al., Satellite and correlative measurements of the stratospheric aerosol, II, Comparison of measurements made by SAM II, dustsondes and an airborne lidar, *J. Atmos. Sci.*, **38**, 1295-1312, 1981.
- Schnetzler, C. G., G. J. S. Bluth, A. J. Krueger, L. S. Walter, and S. Doiron, A sulfur emission index (SEI) for explosive volcanic eruptions, (abstract), *Eos Trans. AGU*, Fall Meeting Suppl., 614, 1992.
- Schoeberl, M. R., P. K. Bhartia, and E. Hilsenrath, Tropical ozone loss following the eruption of Mt. Pinatubo, *Geophys. Res. Lett.*, **20**, 29-32, 1993.
- Smithsonian Institution, *Global Volcanism 1975-1985*, edited by L. McClelland, T. Simkin, M. Summers, E. Nielsen, and T. C. Stein, 657 pp., Prentice-Hall, Englewood Cliffs, N. J., 1989.
- Stolarski, R. S. and H. Wesoky (Eds.), The atmospheric effects of stratospheric aircraft: A second program report, *NASA Ref. Publ. 1293*, 233 pp., Office of Space Sci. and Appl., Washington, D. C., 1993.
- Telegadas, K., and R. J. List, Are particulate radioactive tracers indicative of stratospheric motions?, *J. Geophys. Res.*, **74**, 1339-1350, 1969.
- Thomason, L. W., and L. R. Poole, On the use of Antarctic stratospheric aerosol properties as diagnostics of vortex processes, *J. Geophys. Res.*, **98**, 23,003-23,012, 1993.
- Trepte, C. R., Tracer transport in the lower stratosphere, Ph.D. dissertation, 169 pp., Univ. of Wis. - Madison, 1993.
- Trepte, C. R., and M. H. Hitchman, Tropical stratospheric circulation deduced from satellite aerosol data, *Nature*, **335**, 626-628, 1992.
- Trepte, C. R., R. E. Veiga, and M. P. McCormick, The poleward dispersal of Mount Pinatubo volcanic aerosol, *J. Geophys. Res.*, **98**, 18,563-18,573, 1993.
- Tuck, A. F., J. M. Russell III, and J. H. Harries, Stratospheric dryness: Antiphased desiccation over Micronesia and Antarctica, *Geophys. Res. Lett.*, **20**, 1227-1230, 1993.
- Turco, R. P., P. Hamill, O. B. Toon, R. C. Whitten, and C. S. Kiang, A one-dimensional model describing aerosol formation and evolution in the stratosphere, I, Physical processes and mathematical analogs, *J. Atmos. Sci.*, **36**, 699-717, 1979.
- Wilson, E. O., *The Diversity of Life*, W. W. Norton, New York, 424 pp., 1992.
- Yulaeva, E., J. R. Holton, and J. M. Wallace, On the cause of the annual cycle in tropical lower stratospheric temperatures, *J. Atmos. Sci.*, **51**, 169-174, 1994.

Zhang, C., On the annual cycle in highest, coldest clouds in the tropics, *J. Clim.*, *6*, 1987-1990, 1993.

son, WI 53706. (e-mail: matt@adams.meteor.wisc.edu; megan@adams.meteor.wisc.edu; chip@mirage.larc.nasa.gov)

M. H. Hitchman, M. McKay, and C. R. Trepte, Department of Atmospheric and Oceanic Sciences, University of Wisconsin - Madison, 1225 W. Dayton Street, Madi-

(Received July 26, 1993; revised June 7, 1994; accepted June 13, 1994.)